Liquid Crystals
Publication details, including instructions for authors and subscription information:
http://www.informaworld.com/smpp/title~content=t713926090

Dielectric spectroscopy of unsymmetrical liquid crystal dimers showing wide temperature range TGBA and TGBC* phases

Abhay S. Pandey[a]; R. Dhar[ab]; M. B. Pandey[b]; A. S. Achalkumar[c]; C. V. Yelamaggad[c]
[a] Material Research Laboratory, Physics Department, Ewing Christian College, Allahabad University, Allahabad-211 003, India [b] Physics Department, Allahabad University, Allahabad-211 002, India [c] Centre for Liquid Crystal Research, Jalahalli, Bangalore-560 013, India

To cite this Article Pandey, Abhay S. , Dhar, R. , Pandey, M. B. , Achalkumar, A. S. and Yelamaggad, C. V.(2009) 'Dielectric spectroscopy of unsymmetrical liquid crystal dimers showing wide temperature range TGBA and TGBC* phases', Liquid Crystals, 36: 1, 13 — 19
To link to this Article: DOI: 10.1080/02678290802638415
URL: http://dx.doi.org/10.1080/02678290802638415

Liquid Crystals,
Vol. 36, No. 1, January 2009, 13–19

Taylor & Francis
Taylor & Francis Group

Dielectric spectroscopy of unsymmetrical liquid crystal dimers showing wide temperature range TGBA and TGBC* phases

Abhay S. Pandey[a], R. Dhar[ab]*, M. B. Pandey[b], A. S. Achalkumar[c] and C. V. Yelamaggad[c]

[a]*Material Research Laboratory, Physics Department, Ewing Christian College, Allahabad University, Allahabad-211 003, India;* [b]*Physics Department, Allahabad University, Allahabad-211 002, India;* [c]*Centre for Liquid Crystal Research, Jalahalli, Bangalore-560 013, India*

(Received 30 September 2008; in final form 20 November 2008)

The electrical properties of frustrated twist grain boundary (TGB) phase are a matter of curiosity. Some studies have indicated the existence of soft and Goldstone modes in TGBA and TGBC* phases respectively. However, the experimental results are still not very conclusive. In the present work, we report dielectric studies of wide temperature range TGBA and TGBC* phases of an optically active dimeric compound 4-*n*-decyloxy-4′-(cholesteryloxycarbonyl-1-butyloxy) chalcone in the frequency range of 1 Hz to 35 MHz for the planar and homeotropic anchoring of the molecules. Two different relaxation processes have been detected for the planar anchoring of molecules in the TGBA and TGBC* phases. The soft mode like behaviour is obtained due to tilt fluctuation of molecules in the megahertz region for both TGBA and TGBC* phases. Goldstone mode like behaviour due to phase fluctuation of molecules has been detected for the TGBC* phase in the low frequency region (~200–300 Hz). Activation energies for DC conductivity have also been determined for various phases of the material.

Keywords: TGB phases; dielectric permittivity and anisotropy; dielectric strength; relaxation frequency; ionic conductivity.

1. Introduction

Two decades ago, a novel liquid crystal phase consisting of chiral molecules was theoretically predicted by Renn and Lubensky (*1*) on the basis of analogy between the liquid crystalline smectic A (SmA) phase and superconductors. The predicted phase was equivalent to the Abrikosov flux lattice phase of type-II superconductors in an external magnetic field (*1, 2*). It consists of twisted SmA slabs mediated by grain boundaries of parallel screw dislocation, hence it is called twist grain boundary A (TGBA) phase. The first experimental observation of a TGBA phase was reported by Goodby et al. (*3, 4*). While the structure of the TGBA phase seems to be quite well understood, the character and properties of its tilted variants (TGBC and TGBC*) are still the subject of intense debate (*5*). The first example of the corresponding TGBC* phase was published by Nguyen et al. (*6*). The relationship between the molecular structure and formation of the TGB phases is still unknown and a systematic study of physical properties is needed to ascertain the formation of these frustrated phases. However, on the basis of various studies, the presence of the frustrated phases is associated with the high twisting power. Dielectric studies of the TGB phases are still scarce, because in most of the systems TGB phases exist over a very short temperature range due to their frustrated nature. So far, only a few literature data are available on the dielectric behaviour of TGB phases (*5, 7–14*). Initial frequency dependent (dynamic) dielectric studies of the TGBA phase (*10–12*) show that, like those of SmA* phase, the electric field induces amplitude fluctuation of tilt angle and hence soft mode of dielectric relaxation is observed in the TGBA phase. Similarly in TGBC phase, electric field induces phase fluctuation of the tilt angle and hence the Goldstone mode of dielectric relaxation is observed, like that in the SmC*phase (*7, 13*). However, experimental evidence suggests that TGB phase relaxation processes have lower amplitudes and higher relaxation frequencies as compared with those observed in the classical SmA* and SmC* phases. Ismaili et al. (*7*) have proposed a theoretical model which suggests that the Goldstone mode of TGBC and the soft mode of TGBA are strongly reduced due to the elastic distortion of the director, which results in the existence of an elastic parameter (H_2) in TGB phases. The amplitude of H_2 depends strongly on the anchoring parameter (β_a) arising due to the anchoring forces at the grain boundaries and the distance between the grain boundaries (l_b) in these phases (*7*). However, this theory has not been convincingly verified for general systems possessing various TGB

*Corresponding author. Email: dr_ravindra_dhar@hotmail.com

ISSN 0267-8292 print/ISSN 1366-5855 online

DOI: 10.1080/02678290802638415
http://www.informaworld.com

phases. There are very few systems showing TGB phases in a wide temperature range (*8, 13–15*). Recently, dielectric parameters of exceptionally wide temperature range TGBA and TGBC* phases of unsymmetrical liquid crystal dimer, 4-*n*-undecyloxy-4′- (cholesteryloxycarbonyl-1-butyloxy) chalcone, have been observed and reported (*14*). In this work, we have chosen another member of this homologous series to carry out our investigations, to ascertain expected modes of dielectric relaxation in TGB phases in order to generalise the results.

2. Experimental techniques

The phase transition temperatures and corresponding enthalpies have been obtained by Differential Scanning Calorimetry (DSC) NETZSCH (model DSC 200 F3 Maia). The various phases in the compound have been identified using an optical polarising microscope. The dielectric measurements for the planar aligned sample were carried out in a home-made dielectric cell in the form of a parallel-plate capacitor by using indium tin oxide (ITO) glass plates that have a sheet resistance of less than 25 Ω. Gold coated glass plates of sheet resistance ~1–1.5 Ω have been used for homeotropic aligned cells. Depositing a thin layer of polyamide nylon on electrodes and then rubbing unidirectionally with soft cotton produces planar alignment (long axes parallel to the surface of the electrodes) of the molecules. For homeotropic alignment, the electrodes were coated with lecithin. The material has been filled in the isotropic liquid phase at a temperature of above 10°C to clearing point. Dielectric data have been acquired by using the Newton's Phase Sensitive Multimeter (model-1735) coupled with IAI (model-1257) in the frequency range of 1 Hz to 35 MHz. However, low frequency data have been verified with a Solartron-1260 Impedance analyser coupled with a dielectric interface (model-1296). The temperature of the sample was controlled with the help of a hot stage (Instec model HS-1) having an accuracy of ±0.1°C and resolution of 3 mK. Temperature near the sample has been determined by measuring thermo-emf of a copper-constantan thermo couple with the help of a Agilent six and a half digit multimeter (model-34410A) with the accuracy of ±0.1°C. The active capacitance (C_A) of the cell has been determined by using standard non-polar liquid (cyclohexane in the present case) as follows:

$$C_A = [C(\mathrm{ch}) - C(\mathrm{a})]/[\varepsilon'(\mathrm{ch}) - 1], \tag{1}$$

where C(ch) and C(a) are the capacitance of the cell filled with cyclohexane and air respectively. ε′(ch) is the relative permittivity of cyclohexane. Complete removal of the cyclohexane (after the calibration) from the cell was ensured by comparing the capacity of the cell before and after filling with cyclohexane. The dielectric permittivity and loss of the material have been calculated with the help of formulae as follows:

$$\varepsilon' = [\{C(\mathrm{m}) - C(\mathrm{a})\}/C_A] + 1 \tag{2}$$

and

$$\varepsilon'' = 1/\omega R C_A, \tag{3}$$

where ε′ and ε″ are the dielectric permittivity and loss respectively, C(m) is the capacitance of the cell filled with material, ω is the angular frequency and R is the resistance of the material filled between parallel glass plates.

In the case of dispersive material the measured dielectric spectrum can be described with the help of the following generalised Cole–Cole Equation (*16, 17*).

$$\begin{aligned} \varepsilon^* &= \varepsilon' - j\varepsilon'' \\ &= \varepsilon'(\infty) \\ &+ \sum_i \frac{(\Delta\,\varepsilon)_i}{1 + (j\,\omega\,\tau_i)^{(1-h_i)}} + \frac{A}{\omega^n} - j\frac{\sigma_{ion}}{\varepsilon_0 \omega^k} - jBf^m, \end{aligned} \tag{4}$$

where $\varepsilon'(\infty)$ is the high frequency limiting value of the relative permittivity, $\Delta\varepsilon_i$, τ_i and h_i are the dielectric strength, the relaxation time (inverse of angular relaxation frequency) and the symmetric distribution parameter ($0 \leqslant h_i \leqslant 1$) of the ith mode respectively. The third and fourth terms in Equation (4) represent the contribution of the electrode polarisation capacitance and ionic conductance at low frequencies where A and n are constants (*18*). The fifth imaginary term Bf^m (*19*) is included in Equation (4) partially to account for the high-frequency ITO effect, where B and m are constants since correction terms are small. ε_0 (=8.85 pF m^{-1}) is the free space permittivity. Real and imaginary parts of Equation (4) can be written as:

$$\begin{aligned} \varepsilon' &= \varepsilon'(\infty) \\ &+ \sum_i \frac{\Delta\varepsilon_i \left[1 + (\omega\,\tau_i)^{(1-h_i)} \sin(h_i\pi/2)\right]}{1 + (\omega\,\tau_i)^{2(1-h_i)} + 2(\omega\,\tau_i)^{(1-h_i)} \sin(h_i\pi/2)} \\ &+ \frac{A}{\omega^n} \end{aligned} \tag{5}$$

and

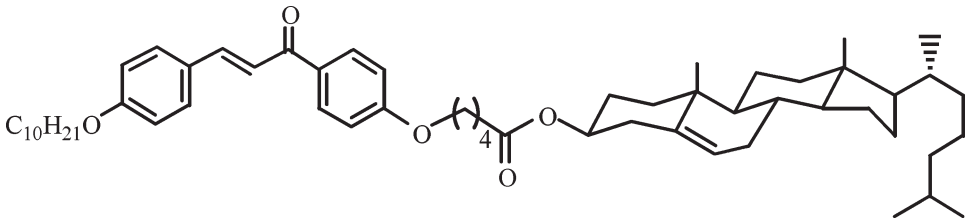

Figure 1. Chemical structure of the compound (4-*n*-decyloxy-4′-(cholesteryloxycarbonyl-1-butyloxy) chalcone) under study.

$$\varepsilon'' = \sum_i \frac{\Delta\varepsilon_i(\omega\,\tau_i)^{(1-h_i)}\cos(h_i\pi/2)}{1+(\omega\,\tau_i)^{2(1-h_i)}+2(\omega\,\tau_i)^{(1-h_i)}\sin(h_i\pi/2)} + \frac{\sigma_{ion}}{\varepsilon_0\omega^k} + Bf^m. \quad (6)$$

To explore the expected mode of relaxation in the present systems, the real part of the dielectric permittivity data has been fitted with the help of Equation (5). After subtracting low frequency correction terms due to electrode polarisation capacitance from the measured data, it has been possible to explore a relaxation phenomenon in TGBA phase at low frequency side.

3. Results and discussion

3.1. Phase transitions

The chemical structure of the investigated compound is shown in Figure 1. Differential Scanning Calorimeter (DSC) thermograms in the heating and cooling cycles of the investigated compound at the scanning rate of 5°C min^{-1} are shown in Figure 2. The investigated compound has the following phase sequences, as obtained by DSC and polarised light microscopic studies.

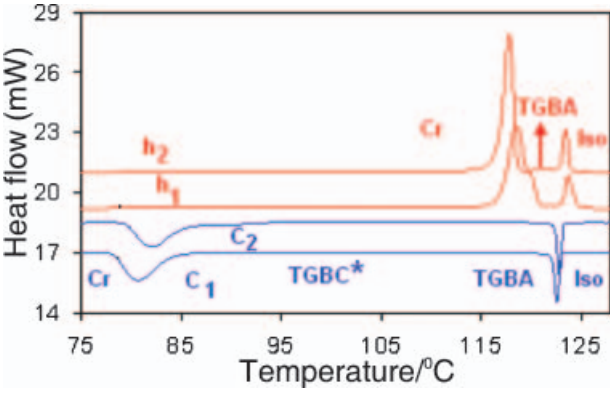

Figure 2. DSC thermograms obtained at the scanning rate of 5.0°C min^{-1} for 4-*n*-decyloxy-4′-(cholesteryloxycarbonyl-1-butyloxy) chalcone. h_1, h_2, first and second heating scans; c_1, c_2, first and second cooling scans.

Heating: Cr118.9°C(46)TGBA 124.4°C(6.8)Iso

Cooling: Iso 123.3°C(6.2)TGBA 104.4°C TGBC*

81.6°C(20.2)Cr

where Iso and Cr stand for isotropic liquid and crystal phase respectively. Data in parentheses are enthalpies (J g^{-1}) whereas those outside the parentheses are transition temperatures (°C) associated with the phase transitions.

The TGBA to TGBC* phase transition was observed under the polarising microscope but was too weak to be recognised on DSC thermograms. The optical textures of TGBA and TGBC* phases are shown in Figure 3. Undulated filaments or a square grid pattern were observed when slides were treated for homeotropic or planar anchoring conditions respectively (*14, 15*). Since the TGBC* phase is monotropic in the studied compound, the dielectric data have been taken in the cooling cycle only.

3.2. Molecular dynamics in the TGBA and TGBC* phases

The measured dielectric permittivity in the homeotropic configuration $(\varepsilon'_{\parallel})$ is almost invariant in the frequency range of 1 kHz to 5 MHz. This rules out any relaxation mechanism due to the individual rotation of the molecules. However, data below 1 kHz suffers from a low frequency parasitic effect (*18*). The measured dielectric permittivity in the planar configuration $(\varepsilon'_{\perp})$ of TGBA phase at 114.0°C is shown in Figure 4. The measured data of $\varepsilon'_{\perp}$ show some decrease for the frequencies above 100 kHz, indicating a pre-dielectric dispersion phenomenon in the frequency range of 100 kHz to 5 MHz (see Figure 4). As the temperature goes down, this mechanism further dominates. From Figure 4, one can see that, when going from 10 kHz to 3 MHz, $\varepsilon'_{\perp}$ decreases by ~0.23 (at 114°C). This indicates that the dielectric strength of the expected relaxation mode is very weak. Due to weak dielectric strength and dominance of high frequency correction term, we could not detect experimentally the peak of the dielectric loss curve.

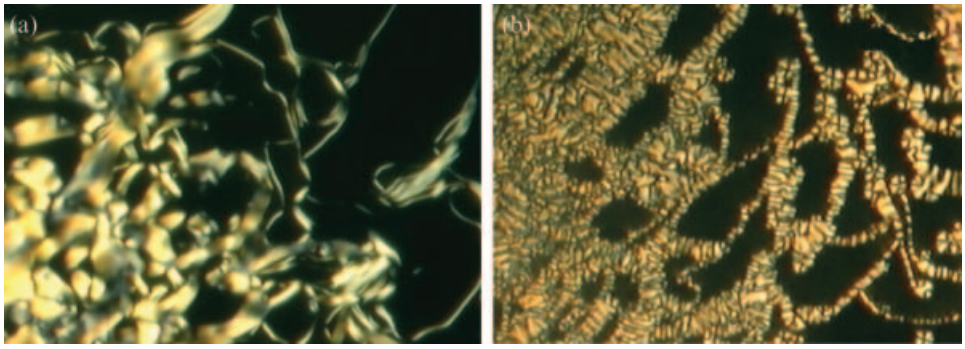

Figure 3. Optical textures observed for 4-*n*-decyloxy-4′-(cholesteryloxycarbonyl-1-butyloxy) chalcone on slides treated for homeotropic orientation: (a) filaments of TGB growing from the isotropic liquid at 122.0°C; (b) undulated filaments of TGBC* phase at 100.0°C.

It is important to mention here that high frequency effects start at least one decade lower in the dielectric loss in comparison with the dielectric permittivity curve. The dielectric loss in the investigated compound is very small (~0.1 at 114.0°C and 100 kHz frequency) and it increases with frequency at least four-fold between 100 kHz and 1 MHz due to the dominance of parasitic effects. Hence, experimentally it is not feasible to determine the peak of the loss curve, for which the maximum is $\sim\Delta\varepsilon/2$. At the TGBA–TGBC* transition, high frequency values of $\varepsilon'_{\perp}$ move further down (see Figure 5). It is apparent from Figures 4 and 5 that the observed mode of the TGBA phase continues in the TGBC* phase as well, with an increase in its strength. The dielectric strength of this mode has been found to be ~1.10 at 94.0°C. To obtain the temperature dependency of the relaxation frequency corresponding to the observed

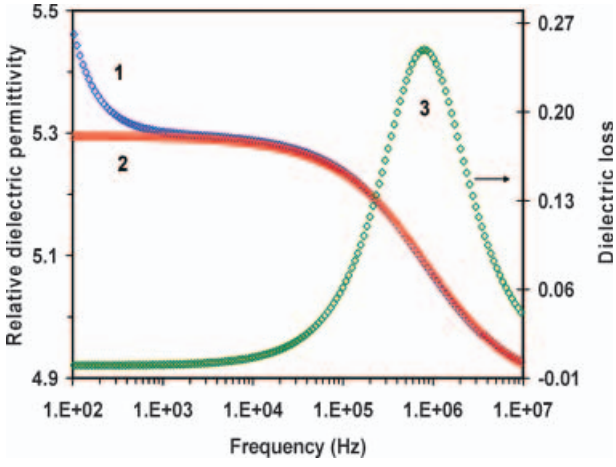

Figure 4. Variation of the measured relative dielectric permittivity (with fit of Equation (5) on the experimental data) by curve 1 and corrected data (measured data-parasitic effects) by curve 2 and dielectric loss (generated with the use of Equation (6)) by curve 3 with frequency for the TGBA phase (114.0°C) showing soft mode-like relaxation.

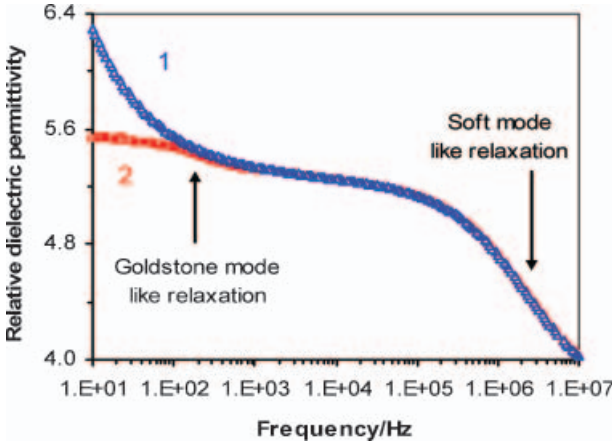

Figure 5. Variation of relative dielectric permittivity (with fit of Equation (5) on the experimental data) by curve 1 and corrected data (measure data-parasitic effects) by curve 2 with frequency for the TGBC* phase (94.0°C).

mode, the experimental dielectric permittivity curve has been fitted with Equation (5) and the results are shown in Figure 6. It has been observed that the relaxation frequency follows Arrhenius behaviour as follows:

$$f_r = f_0 \exp(-Wa/NkT) \tag{7}$$

where T is the temperature in K, N is the Avogadro number, k $(=1.38\times10^{-23}\,\mathrm{J\,K^{-1}})$ is the Boltzmann constant and Wa is the activation energy. We found the activation energy for TGBA and TGBC* phases to be $45.5\,\mathrm{kJ\,mol^{-1}}$ and $56.3\,\mathrm{kJ\,mol^{-1}}$, respectively (see Figure 6).

Now we come to the expected origin of the observed mode. A dielectric mode due to the rotation around a short axis is observed in the low megahertz region of the classical smectic (SmA and SmC) phases. At the SmA to SmC transition, either slope changes or a jump in the relaxation frequency is seen due to a change in the potential barrier of two phases.

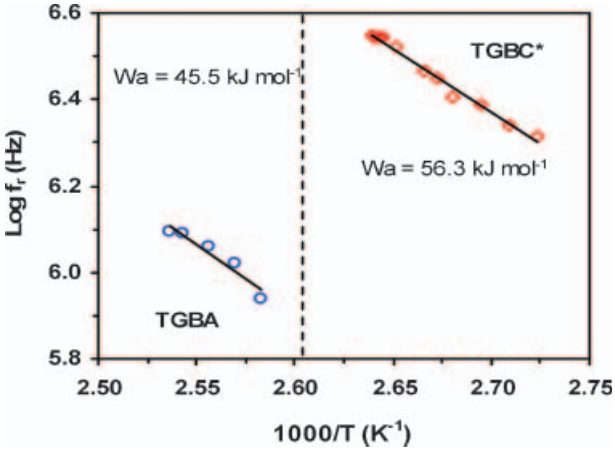

Figure 6. The Arrhenius plots for relaxation frequencies observed in the TGBA and TGBC* phases for the compound 4-*n*-decyloxy-4′- (cholesteryloxycarbonyl-1-butyloxy) chalcone.

However, in the present case, the relaxation frequency of the observed mode is increasing at the TGBA to TGBC* transition, which is contrary to the classical SmA to SmC transition. More so, this mode is not observed for homeotropic oriented samples. Hence the rotation around a short axis as a possible origin of this mode is ruled out. On the other hand, existence of the soft mode in TGB phases has been theoretically predicted and experimentally detected in this frequency range (*7, 8*). The dielectric strength of the present mode also increases on lowering the temperature. This indicates the collective nature of the mode. Hence, we assign this weak relaxation mode as the soft mode of TGBA and TGBC* phases of the present material.

From Figure 7, one can see that the value of $\varepsilon'_{\perp}$ increases (below 1 kHz) upon cooling. This indicates

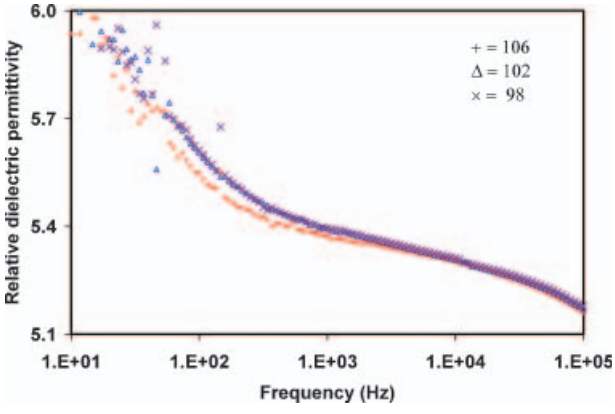

Figure 7. Frequency dependence of the relative dielectric permittivity at 98.0°C and 102.0°C (TGBC* phase) and at 106.0°C (TGBA phase), which shows the emergence of another mode on the low frequency side of the TGBC* phase.

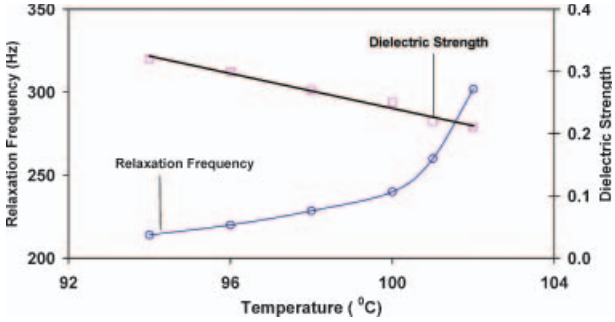

Figure 8. Temperature dependence of the relaxation frequency and dielectric strength for the Goldstone-like mode in the TGBC* phase.

the presence of another collective relaxation mechanism in this phase between 10 Hz and 1 kHz; however, data below 100 Hz are affected due to low frequency parasitic contributions. To explore the behaviour of the expected low frequency mode, dielectric dispersion curves have been fitted with Equation (5). After subtracting electrode polarisation effects, low frequency mode is clearly visible in the TGBC* phase (Figure 4). The temperature dependence of relaxation frequency and dielectric strength of this mode of TGBC* phase is shown in Figure 8. The relaxation frequency and dielectric strength of this mode are invariant with temperature. Hence we assign this low frequency mode as the Goldstone-like mode of the TGBC* phase of the present material.

3.3. Dielectric anisotropy of the TGBA and TGBC phases*

Variations of $\varepsilon'_{\perp}$ and $\varepsilon'_{\parallel}$ (100 Hz), indicating variation of the dielectric anisotropy $\left(\Delta\varepsilon' = \varepsilon'_{\parallel} - \varepsilon'_{\perp}\right)$ with the temperature, is shown in Figure 9. As expected, in

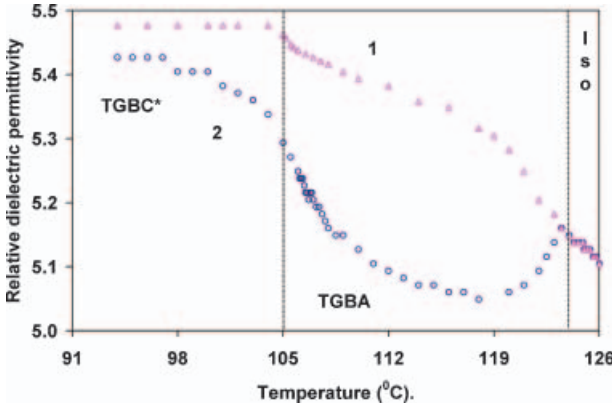

Figure 9. Variation of relative dielectric permittivity for planar (curve 1) and homeotropic (curve 2) aligned samples with temperature at 100 Hz, indicating dielectric anisotropy ($\Delta\varepsilon'$) with the temperature. Vertical lines show the transition temperatures on the basis of dielectric studies.

the isotropic liquid phase $\Delta\varepsilon'$ has been found to be ~ 0, showing that there is no preferred alignment of the molecules. Below the isotropic liquid to TGBA transition temperature ($T_{\text{I-TGBA}}$), $\varepsilon'_{\perp}$ increases (whereas $\varepsilon'_{\parallel}$ decreases sharply) with a decrease in the temperature, showing negative dielectric anisotropy $\left(\Delta\varepsilon' = \varepsilon'_{\parallel} - \varepsilon'_{\perp} < 0\right)$ in the TGBA phase.

Good planar alignment has not been achieved immediately below $T_{\text{I-TGBA}}$, but as temperature decreases in the TGBA phase, molecular alignments improve and that is why $\varepsilon'_{\perp}$ increases slowly in the vicinity of the isotropic liquid to TGBA transition. A clear change in slope of $\varepsilon'_{\perp}$ has been observed at $\sim 105^{\circ}$C. This suggests macroscopic change in the structure of material at this temperature and confirms the existence of another phase below this temperature, which has also been observed during the polarised light microscopic study as well. As mentioned earlier, the observed square grid texture for the homogeneously (planar) aligned samples confirms this phase as TGBC* (*15*).

At the TGBA to TGBC* transition, $\varepsilon'_{\parallel}$ jumps up by an appreciable magnitude. Increase in the value of $\varepsilon'_{\parallel}$ at the TGBA to TGBC* transition can be assigned to the tilt of molecules in the smectic blocks. Such behaviour has been observed in some other, similar, systems also (*13, 14*). In the TGBA phase, molecules are always normal to the smectic layers. Hence, with the rotation of smectic blocks and hence layer planes (along the TGB helix), molecules are also rotated and no longer normal to the bounding surfaces. In the TGBC* phase, rotating smectic blocks are filled with tilted helical SmC structure in such a way that the helix of the SmC* structure is always normal to the TGB helix. Hence it is just possible that molecules of many more TGB blocks (compared with the TGBA phase) are normal to the electrode surfaces (due to surface anchoring forces), whereas the blocks and hence smectic layers are rotated by approximately the tilt angle. This causes an increase in the longitudinal component of the permittivity $\left(\varepsilon'_{\parallel}\right)$ at the TGBA to TGBC* transition.

3.4. *Ionic conductivity of the TGBA and TGBC* phases*

Ionic conductivity (σ(ion)) has been determined from the measured conductivity data in different phases of the investigated compound for planar and homeotropic alignments of the sample. For the planar oriented sample, it has been observed that ionic conductivity ($\sigma_{\perp}$(ion)) marginally increases at the isotropic liquid to TGBA transition (see Figure 10). $\sigma_{\perp}$(ion) continuously decreases with the decrease in the temperature throughout the TGBA and TGBC* phases and follows Arrhenius behaviour. This can be attributed to an increase in the viscosity of the material with the decrease in the temperature. The values of $\sigma_{\perp}$(ion) in the isotropic liquid and TGBA phases are of the order of $10^{-8}\,\text{S m}^{-1}$ and go down to $10^{-9}\,\text{S m}^{-1}$ on the lower temperature side of the TGBC* phase. No sharp change in the value of $\sigma_{\perp}$(ion) has been observed at the TGBA to TGBC* transition but a change of slope distinguishes two phases (see Figure 10). The activation enthalpy of ionic-conductivity has been calculated in different phases using the following relation:

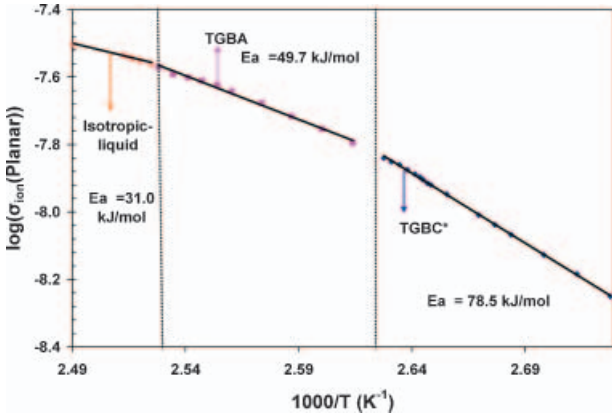

Figure 10. Variation of ionic conductivity with temperature in various phases of the compound for the planar aligned sample.

$$\sigma = \sigma_0 \exp\left(-\frac{Ea}{NkT}\right), \tag{8}$$

where σ_0 is a constant and *Ea* is the activation energy of ionic conductivity.

The values of activation energy in the isotropic liquid, TGBA and TGBC* phases are found to be $31.0\,\text{kJ mol}^{-1}$, $49.7\,\text{kJ mol}^{-1}$ and $78.5\,\text{kJ mol}^{-1}$, respectively. The activation energy in the TGBC* phase is found to be approximately one and a half times that of the TGBA phase. It is supposed that the movements of the free ions are more restricted due to the tilting of smectic blocks in the low temperature TGBC* phase.

When electrodes are treated for homeotropic anchoring (coated with lecithin) it has been observed that σ(ion) increases by at least one order of magnitude even in the isotropic liquid phase. This has been the usual process in various types of materials studied by us where lecithin has been used as the surfactant. It seems that lecithin molecules contribute to ionic conductance by injecting extra impurity ions, otherwise σ(ion) must be the same in both types of cell (planar and homeotropic) in the isotropic liquid phase of the samples as there must not be any preferred alignment of the molecules. For this reason ionic conductivity could not be determined precisely in the homeotropic aligned sample.

4. Conclusions

Thermodynamic, optical texture and dielectric studies prove the existence of wide temperature range TGBA and TGBC* phases in the investigated compound. A relaxation process in the frequency range of 100 kHz to 5 MHz has been observed in both the TGBA and TGBC* phases, presumably due to the soft mode behaviour. Another weak mode of relaxation has been detected in the TGBC* phase at around 200 Hz and it has the signature of the Goldstone mode. In the present study, we have succeeded in detecting these dielectric relaxation modes in the wide temperature range of TGBA and TGBC* phases. However, it is important to mention that characteristics of the observed soft and Goldstone modes are not exactly the same as in the corresponding modes of SmA* and SmC* systems.

Acknowledgements

We thank the Department of Science of Technology (DST), New Delhi for financial support under a research project. ASP thanks the DST for fellowship under the project. RD thanks the University Grants Commission, New Delhi for leave from teaching lead under the National Research Award scheme. We are grateful to Professor I.M.L. Das, In-charge Impedance Spectroscopy Laboratory, and Professor Pradip Kumar (Head), Physics Department, Allahabad University for providing low frequency dielectric measurement facilities.

References

(1) Renn S.R.; Lubensky T.C. *Phys. Rev. A* **1988**, *38*, 2132–2147.
(2) Renn S.R.; Lubensky T.C. *Mol. Cryst. Liq. Cryst.* **1991**, *209*, 349–355; Renn S.R. *Phys. Rev. A* **1992**, *45*, 953–973.
(3) Goodby J.W.; Waugh M.A.; Stein S.M.; Chin E.; Pindak R.; Patel J.S. *Nature* **1989**, *337*, 449–452.
(4) Goodby J.W.; Waugh M.A.; Stein S.M.; Chin E.; Pindak R.; Patel J.S. *J. Am. Chem. Soc* **1989**, *111*, 8119–8125.
(5) Novotna V.; Kaspar M.; Hamplova V.; Glogarova M.; Bilkova P.; Domenici V.; Pociecha D. *Liq. Cryst.* **2008**, *35*, 287–298.
(6) Nguyen H.T.; Bouchta A.; Navailles L.; Barois P.; Isaert N.; Twieg R.J.; Maroufi A.; Destrade C. *J. Physique II* **1992**, *2*, 1889–1906.
(7) Ismaili M.; Bougrioua F.; Isaert N.; Legrand C.; Nguyen H.T. *Phys. Rev. E* **2001**, *65*, 011701–1–15.
(8) Gupta M.; Dhar R.; Agrawal V.K.; Dabrowski R.; Tykarska M. *Phys. Rev. E* **2005**, *72*, 021703–1–10; Dhar R. *Phase Transitions* **2006**, *79*, 175–199.
(9) Kaspar M.; Bilkova P.; Bubnov A.; Hamplova V.; Novotna V.; Glogarova M.; Knizek K.; Pociecha D. *Liq. Cryst.* **2008**, *35*, 641–651.
(10) Girold C.; Legrand C.; Isaert N.; Pochat P.; Parneix J.P.; Nguyen H.T.; Destrade C. *Ferroelectrics* **1993**, *147*, 171–179.
(11) Wrobel S.; Hiller S.; Pfeiffer M.; Marzec M.; Haase W. *Liq. Cryst.* **1995**, *18*, 21–29.
(12) Bougrioua F.; Isaert N.; Legrand C.; Bouchta A.; Barois P.; Nguyen H.T. *Ferroelectrics* **1996**, *180*, 35–48.
(13) Pandey M.B.; Dhar R.; Kuczynski W. *Ferroelectrics* **2006**, *343*, 69–82.
(14) Pandey M.B.; Dhar R.; Achalkumar A.S.; Yelamaggad C.V. *J. Phys. Condens. Matter* **2007**, *19*, 436219–1–12; Pandey M.B.; Dhar R.; Achalkumar A.S.; Yelamaggad C.V. *Phase Transitions* **2008**, *81*, 449–458.
(15) Yelamaggad C.V.; Achalkumar A.S.; Bonde N.L.; Prajapati A.K. *Chem. Mater.* **2006**, *18*, 1076–1078.
(16) Cole K.S.; Cole R.H. *J. Chem. Phys.* **1941**, *9*, 341–351.
(17) Pandey M.B.; Dhar R.; Agrawal V.K.; Khare R.P.; Dabrowski R. *Phase Transitions* **2003**, *76*, 945–958.
(18) Srivastava S.L.; Dhar R. *Indian J. Pure Appl. Phys.* **1991**, *29*, 745–751.
(19) Srivastava S.L. *Proc. Nat. Acad. Sci. India* **1993**, *63*, 311–332; Dhar R. *Indian J. Pure Appl. Phys*. **2004**, *42*, 56–61.